INTEGRATED ENGINE-CYCLE AND STRUCTURAL MODELLING FOR REUSABLE LIQUID ROCKET ENGINES

Mateusz T. Gulczyński (1, 2), Jan Deeken (1, 2)

(1) German Aerospace Research Center (DLR), Institute of Space Propulsion, Hardthausen am Kocher, Germany
(2) RWTH Aachen University, Faculty of Mechanical Engineering, Aachen, Germany
Email: Mateusz.Gulczynski@dlr.de

KEYWORDS: combustion chamber, design-oriented modelling, engine-cycle simulation, fatigue life prediction, multidisciplinary coupling, reusability, thermo-structural analysis

ABSTRACT:

Designing reusable liquid rocket engines requires early-stage methods that consistently link engine-cycle modelling with structural durability assessment. Engine-cycle simulations provide essential performance insight, yet their direct implications for the fatigue life of critical components across the full operational envelope remain insufficiently quantified. Consequently, methods are needed that are efficient to apply while maintaining the accuracy required to resolve the mechanisms that drive failure.

This study presents an integrated modelling framework that couples gas-generator-cycle analysis with thermo-mechanical fatigue assessment of a regeneratively cooled combustion chamber in the ~1 MN thrust class. The cycle is modelled in EcosimPro-ESPSS to obtain transient boundary conditions, which are subsequently applied in an ANSYS-based finite-element model and further evaluated using a previously developed post-processing damage-evolution fatigue method. This combined approach enables time-efficient and precise evaluation by incorporating temperature-dependent material data and a cycle-driven damage formulation to estimate fatigue evolution throughout a representative operating sequence. The results demonstrate how transient thermo-mechanical loading governs damage accumulation and provide a basis for assessing reusability margins and potential operational-envelope adaptations at early design stages.

1. INTRODUCTION

Regeneratively cooled combustion chambers in reusable liquid rocket engines are subjected to extreme thermal and mechanical loading, with heat fluxes approaching 100 MW/m² and gas temperatures above 3600 K. Despite regenerative cooling, the resulting thermal and pressure gradients induce cyclic plastic deformation in the inner liner, leading to progressive fatigue damage and ultimately limiting component lifetime, particularly in the throat region [1–5]. Fig. 1 illustrates a representative engine configuration, highlighting the throat region as the primary failure location, where cyclic plastic strain promotes structural degradation, including localised bending (dog-house effect) and eventual ligament rupture. In the throat region, the structural response is governed by the interaction between engine operating conditions and local thermo-mechanical loading [6–10], which determines damage accumulation and the achievable lifetime of the combustion chamber [5–8,11,12]. Evaluation of these effects during engine operation is typically based on engine cycle simulations and component-level structural analyses performed independently, limiting consistent lifetime assessment under transient conditions. The lack of direct integration between system-level engine cycle models and detailed thermo-structural analyses remains a key limitation [13–22]. To overcome this gap, a framework is developed that integrates fatigue life evaluation into transient engine-cycle simulations through post-processing, enabling consistent propagation of operating conditions into structural damage prediction while reducing computational effort.

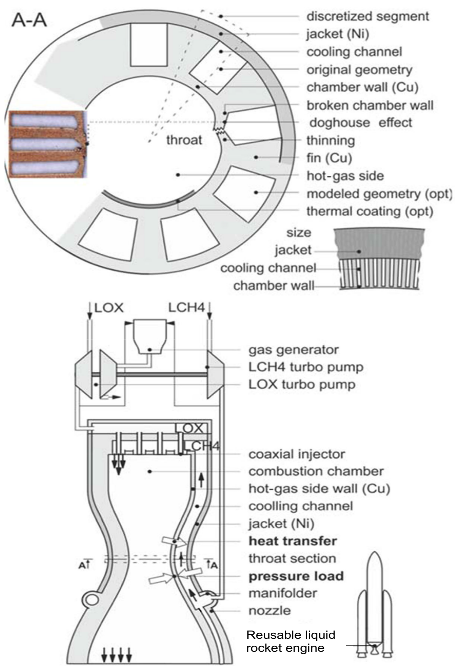

Figure 1 Reusable liquid rocket engine configuration with a regeneratively cooled combustion chamber, highlighting the throat region and failure location

2. METHODOLOGY

To enable integrated component- and system-level analyses, a high-fidelity liquid rocket engine (LRE) model was developed in the EcosimPro environment. The selected configuration corresponds to a high-thrust Vulcain 2-class gas generator (GG) cycle engine, with key parameters derived from literature. The model is coupled with a previously developed and validated fatigue life framework, as presented in [6–8]. It employs finite element analysis (FEA) and post-processing techniques for critical damage evaluation and life prediction in the combustion chamber liner. The employed methodology is illustrated in Fig. 2.

The transient engine cycle captures ignition, start-up, steady-state operation, and shutdown, representing the dominant thermo-mechanical load variations governing fatigue of regeneratively cooled combustion-chamber walls [23–26]. The resulting thermodynamic and flow variables, including wall heat flux, heat-transfer coefficient, coolant pressure, and bulk coolant temperature, are transferred via a MATLAB interface and applied as boundary conditions to the combustion chamber finite element model in ANSYS. For the subsequent thermal–structural analysis, the steady-state phase is extended to 540 s, consistent with the nominal combustion duration, to approximate realistic high-temperature exposure and resulting wall temperature and stress evolution [27,28]. This enables automated coupling between engine cycle simulation and structural analysis, ensuring consistent transfer of transient loads without empirical scaling. The resulting thermo-mechanical histories are post-processed to determine damage accumulation and the critical life of the combustion chamber wall.

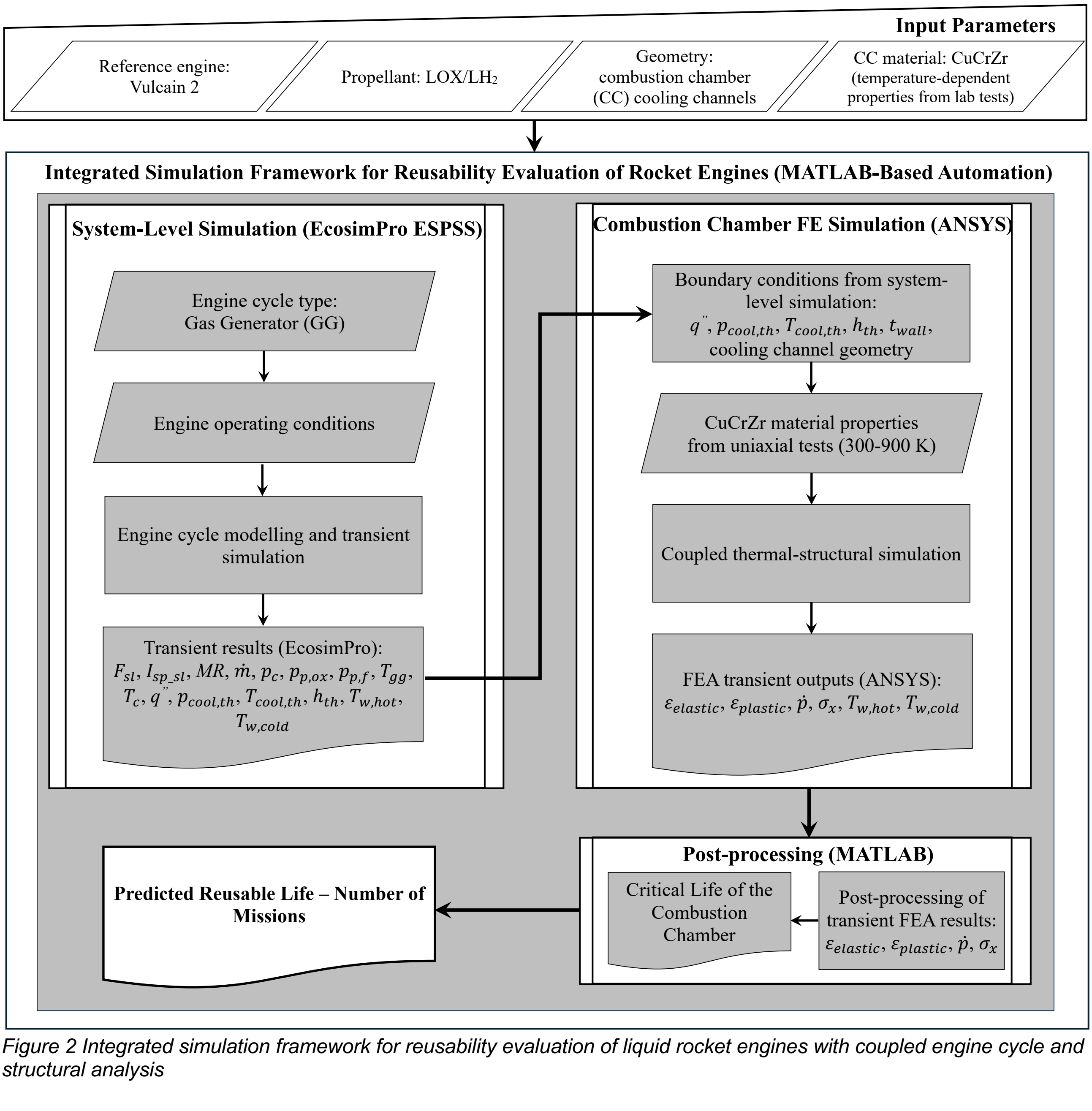

Figure 2 Integrated simulation framework for reusability evaluation of liquid rocket engines with coupled engine cycle and structural analysis

2.1. System- Level Simulation EcosimPro ESPSS

The gas-generator (GG) cycle model follows the architecture of a Vulcain-2-class LOX/LH_2 engine operating at sea-level conditions, as illustrated in Fig. 3. Liquid oxygen (LOX) and liquid hydrogen (LH_2) are supplied from the feed tanks (LOX_supply, LH2_supply) through the oxidiser and fuel inlet valves (VAO, VAH). Each propellant is pressurised by a dedicated turbopump (Pump_O for LOX, Pump_H for LH_2) mechanically driven by its corresponding turbine (Turb_O, Turb_H). The turbines are driven by hot gas generated in the fuel-rich gas generator (Gas_generator), which provides the mechanical energy required to drive the pumps.

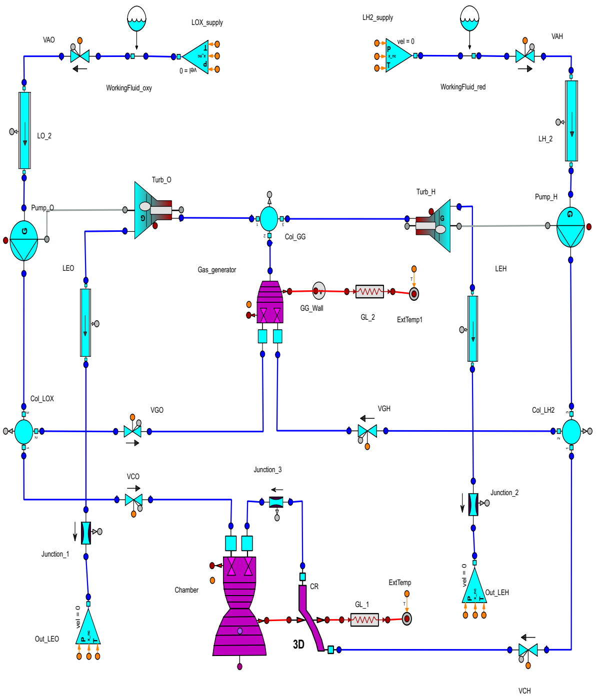

Figure 3 Gas generator cycle engine model schematic for a Vulcain-2-class configuration

Downstream of the oxidiser pump, the liquid-oxygen flow divides into two branches: the main stream passes through the oxidiser control valve (VCO) and feed line (Col_LOX) to the combustion chamber, while the secondary branch supplies the gas generator via the oxidiser valve (VGO). The liquid-hydrogen circuit follows an analogous configuration, with one fraction directed to the gas generator through the fuel valve (VGH) and the remainder routed through the main fuel control valve (VCH) into the feed line (Col_LH_2). The coolant flow circulates through the regeneratively cooled combustion-chamber channels (CR), where it absorbs heat from the hot-gas-side wall, thereby maintaining the structural integrity of the copper liner and preheating the hydrogen to improve atomisation and combustion stability within the chamber [23].

The simulation resolves the key thermodynamic and fluid-dynamic interactions governing engine operation, including the coupling between propellant mass flow, mixture ratio, and chamber pressure throughout the firing sequence. From the time-resolved results, quantities relevant for thermo-structural and fatigue evaluation are extracted, such as the throat heat-transfer coefficient, wall heat flux, coolant pressure, bulk temperature, mass-flow rate and effective wetted area. These data provide the transient thermal and mechanical boundary conditions for the subsequent finite-element thermo-structural analysis in ANSYS and the post-processing method, representing the regeneratively cooled combustion chamber.

Fig. 4 presents the time-resolved response of the simulated engine, showing the evolution of thrust, mixture ratio, specific impulse, mass-flow rates, combustion-chamber pressure, and pump outlet pressures throughout the firing sequence, including ignition, start-up, steady-state operation, and shutdown. The thrust increases from ignition at 1.98 s, reaching 960 kN by 2.36 s, and remains stable during the main burn with fluctuations below ±0.3 %. Shutdown begins at 6.00 s, followed by a rapid decay as the valves close and propellant flow ceases. The steady-state thrust corresponds to the nominal Vulcain 2 sea-level value of 960 kN [27,29], indicating consistency with the reference thrust level. The specific impulse follows the thrust evolution and stabilises at approximately 345 s once mass-flow equilibrium is reached. The higher value compared with the reported ≈310 s for Vulcain 2 is attributed to simplified boundary conditions and the limited representation of viscous and three-dimensional flow effects in the nozzle and feed-line modelling, which increase the effective expansion efficiency at sea level. The mixture ratio stabilises near 6.7 after start-up, consistent with values reported for the reference engine [27,29]. Minor fluctuations observed before and after the steady-state phase result from asymmetric valve sequencing, in which oxidiser cut-off precedes fuel isolation. This sequence ensures a brief fuel-rich phase during shutdown, which is typical for gas-generator-cycle engines to maintain thermal protection of the critical engine components. These short transients were deemed negligible for the present analysis, as they occur outside the dominant thermal loading interval and are therefore not expected to significantly affect the fatigue-life evaluation.

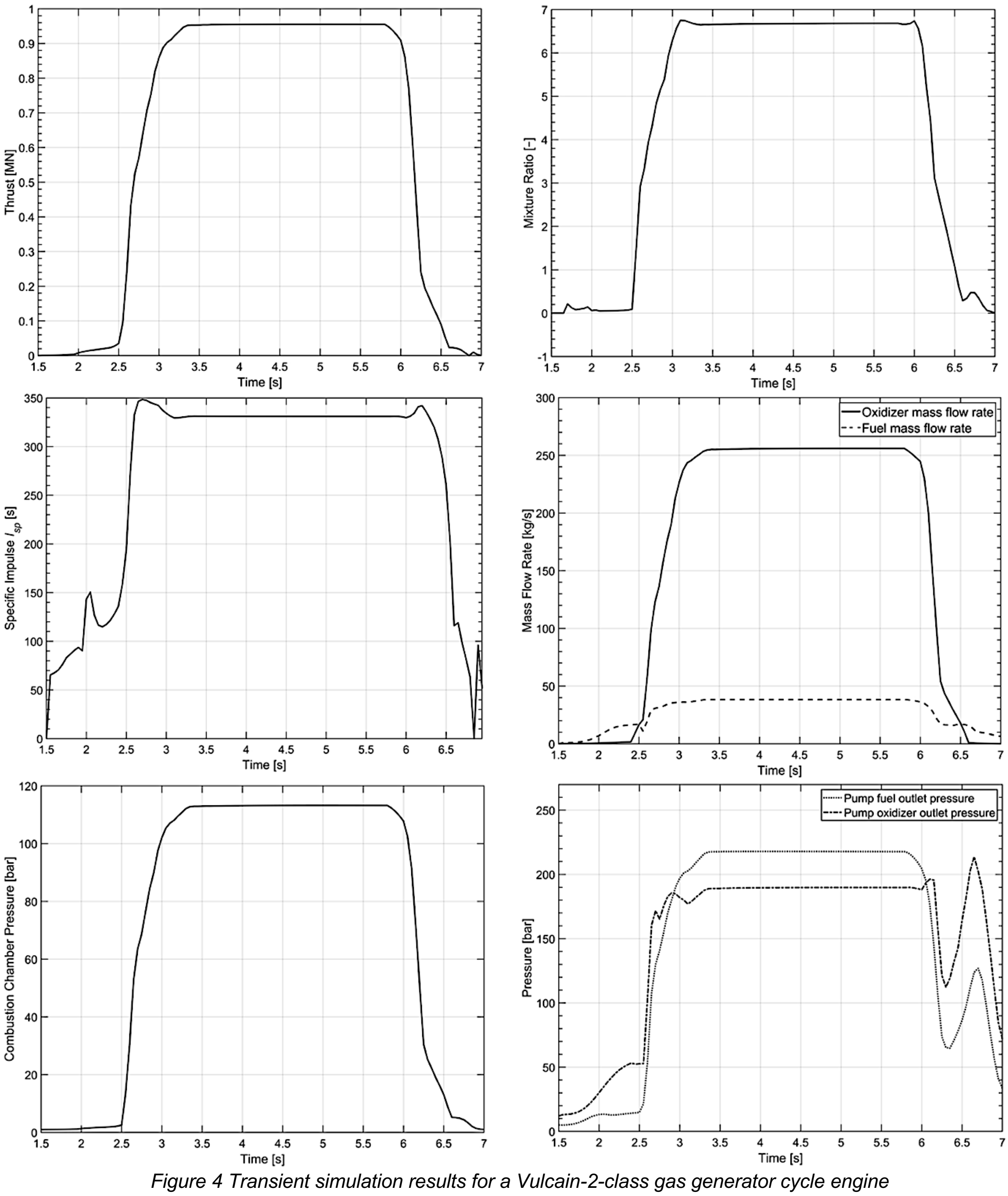

Figure 4 Transient simulation results for a Vulcain-2-class gas generator cycle engine

The oxidiser and fuel mass-flow rates stabilise at approximately 260 kg/s and 40 kg/s, respectively. Following ignition, the combustion-chamber pressure reaches 117 bar, corresponding to the nominal operating regime of this engine class. The attained pressure level determines the turbopump power balance and governs the thermal load imparted to the regeneratively cooled chamber wall. The outlet pressures of the oxidiser and fuel pumps attain approximately 185 bar and 215 bar, respectively, during steady-state operation. These values are governed by the required chamber pressure, propellant mass-flow rates, and the assumed hydraulic losses and turbopump operating conditions in the system-level model. Reported data for the Vulcain 2 engine indicate LOX and LH_2 pump outlet pressures of approximately 154 bar and 182 bar, respectively [29], while an independent source lists a representative turbopump outlet pressure of around 173 bar without specification of the fluid side [30]. The simulated pressures are moderately elevated compared to reference values due to idealised boundary conditions and the omission of minor hydraulic losses in the feed-line modelling. The transient thermodynamic and flow quantities define the boundary conditions for the combustion chamber analysis.

2.2. Combustion Chamber TMF Modelling

The numerical and post-processing combustion chamber models are based on a representative CuCrZr thermo-mechanical fatigue (TMF) panel corresponding to the combustion chamber throat region of a liquid rocket engine and were previously validated against laboratory data [6–8]. Fig. 5, adapted from [6], illustrates the comparison between the experimentally measured panel deformation and the corresponding numerical prediction, showing consistent strain localisation and deformation patterns in the critical region. The validation demonstrated strong agreement between predicted critical life from finite element analysis and experimental results, with deviations below 1% for the tested conditions (~20 MW/m² under representative thermo-mechanical loading). In this study, the finite element formulation and material properties are retained, while the boundary conditions are replaced by engine-cycle-derived thermo-hydraulic loading. This enables critical damage evaluation and direct coupling with system-level operating conditions for reusability assessment.

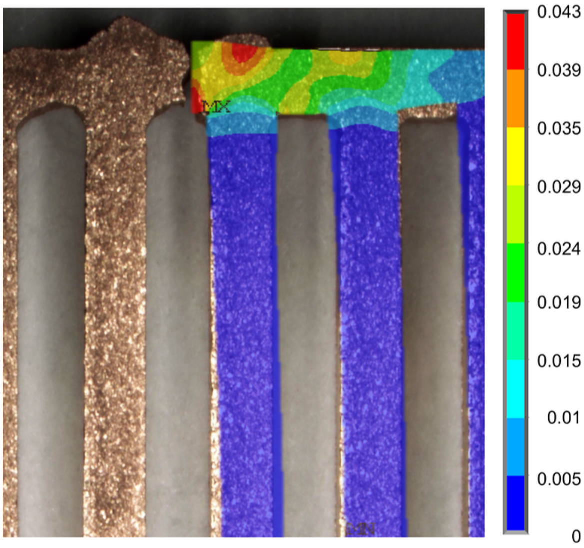

Figure 5 Cross section of the combustion chamber TMF panel showing cooling channels, deformation, and total mechanical strain at the critical location (adapted from [6])

Fig. 6 illustrates the finite element model of the TMF panel, including mesh refinement in the critical region and a representative temperature distribution. The model employs SOLID185 elements, with boundary conditions applied on the surface normal to the X-axis and the inlet surface constrained in the transverse direction of the cooling channels. Nodal coupling ensures consistent temperature and displacement fields in the X- and Z-directions, while a selective integration technique (B-bar method) is used to alleviate incompressible locking and improve correlation with laboratory results. Mesh convergence was verified in the previous study [6], confirming mesh-independent results in the critical regions.

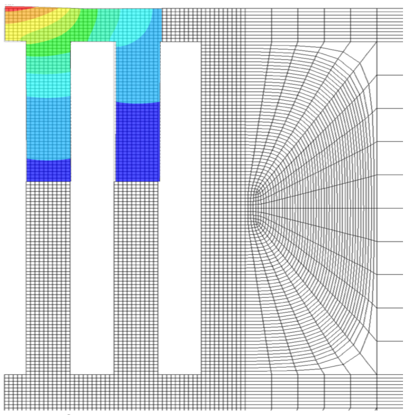

Figure 6 FEM of the TMF panel representing the combustion chamber throat region, including the temperature distribution (≈885 K on the hot-gas side and ≈670 K on the coolant side)

Fatigue life of the combustion chamber wall is evaluated using a damage accumulation framework combining ductile and brittle contributions based on the formulations of Bonora et al. and Dufailly–Lemaitre [31,32]. The evaluation is performed in post-processing using time-resolved variables extracted from finite element simulations, without affecting the stiffness matrix. The variables include equivalent stress, hydrostatic stress, accumulated plastic strain, plastic strain rate, and temperature, with dependencies defined via interpolation between discrete levels. The total damage is defined as the sum of ductile and brittle components:

$$D_{total} = D_{ductile} + D_{brittle} \qquad \text{Eq.1}$$

where the ductile damage component is evaluated as a function of the accumulated strain:

$$D_{ductile} = D_{cr}\left[1 - \left(1 - \frac{\ln\left(\frac{\varepsilon_{(i+1)}}{\varepsilon_{th}}\right)}{\ln\left(\frac{\varepsilon_{f}}{\varepsilon_{th}}\right)}\right)^{\alpha}\right] \qquad \text{Eq.2}$$

and the brittle damage component is determined as:

$$D_{brittle} = \left(\frac{\sigma_{eq,i}^{2} R_{v,i}}{2ES}\right)^{s} \dot{p}_{(t)}\, \Delta t_i \qquad \text{Eq.3}$$

The material parameters and model constants used in Eqs. 2–3 are summarised in Tab. 1.

Table 1 Structural material parameters least-squares fitted from CuCrZr uniaxial fatigue and tensile tests

	Parameter	Unit	300K	700K	900K
Critical damage at the tensile test	D_{cr}	-	0.50	0.38	0.61
Theoretical failure strain	ε_f	-	0.24	0.24	0.16
Damage threshold strain	ε_D (or ε_{th})	-	0.002	0.002	0.0008
Damage exponent	α	-	0.4	0.46	0.14
Material fitting parameters for damage evaluation	S	MPa	49	17	3
	s	-	1	1	1

Damage evolution is governed primarily by cyclic thermo-mechanical loading and associated plastic ratcheting, while material strength degradation is represented using experimentally derived temperature-dependent properties. A critical damage threshold of D_{cr} = 0.61, derived from CuCrZr tests, defines the onset of crack initiation and void formation.

3. RESULTS

The fatigue life of the combustion chamber is evaluated using transient boundary conditions obtained from the EcosimPro engine simulation and applied to the finite element model to determine the resulting thermo-mechanical response of the liner. Fig. 7 shows the corresponding time-resolved boundary conditions. The hot-gas-side heat flux reaches approximately 95 MW/m² during steady-state operation, while the coolant pressure stabilises near 175 bar and the bulk coolant temperature remains within 60–80 K. These values are consistent with reported operating conditions for the Vulcain 2 engine [18,34]. The heat-transfer coefficient follows the transient coolant flow conditions, attaining approximately 175 kW/m²·K. The extracted boundary conditions define the thermo-hydraulic loading for the subsequent thermo-structural fatigue analysis.

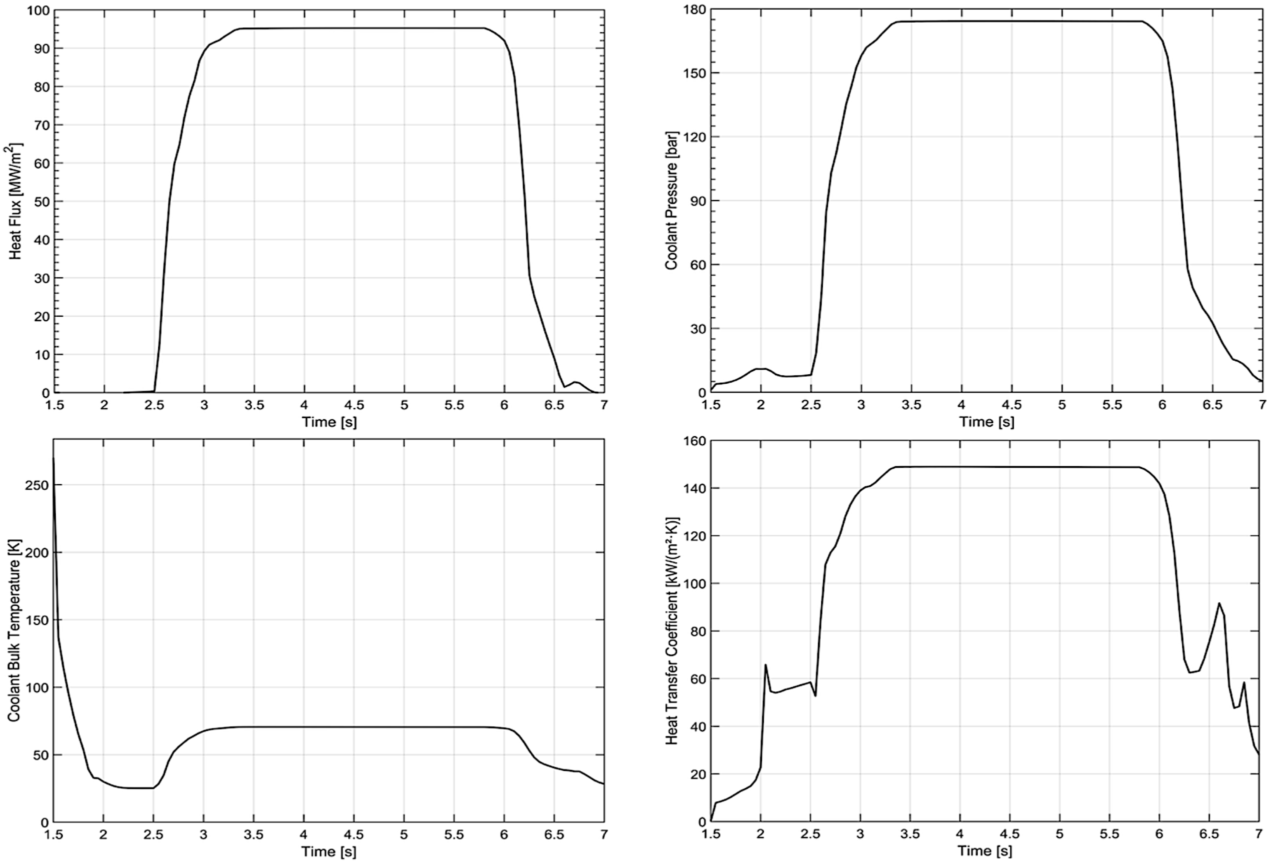

Figure 7 Transient boundary conditions in the throat region of a Vulcain-2-class combustion chamber

Fig. 8 compares the wall-temperature profiles obtained from the EcosimPro engine simulation (left) and the ANSYS finite element analysis (right), with temperatures stabilising near 880 K on the hot-gas side and approximately 670 K on the coolant side during steady operation. The ANSYS temperature distribution, obtained using boundary conditions derived from the EcosimPro simulation, reproduces a similar through-wall gradient. The predicted wall temperatures correspond to reported operating conditions for the Vulcain 2 engine [34].

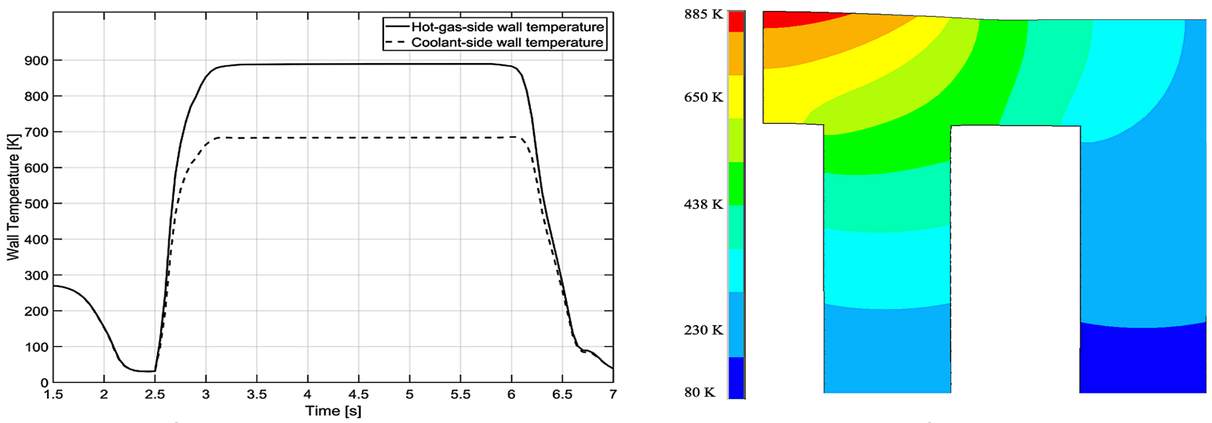

Figure 8 Combustion chamber wall temperature comparison in the throat region for a Vulcain-2-class engine: EcosimPro (left) and ANSYS (right)

The equivalent plastic strain field reveals pronounced plastic strain localisation near the inner radius on the hot-gas side, as illustrated in Fig. 9. This localisation identifies the region of highest inelastic deformation, where the critical damage threshold is first reached.

Figure 9 Equivalent plastic strain distribution in the combustion chamber liner throat region at a representative cycle near failure

Damage evolution in the analysed combustion chamber throat region is presented in Fig. 10. Ductile damage dominates the damage evolution, whereas brittle damage remains negligible throughout the loading history. The critical damage threshold (D_{cr}= 0.61), previously derived from CuCrZr mechanical testing, is reached after 44 load cycles, marking the onset of localised material degradation. The stress–strain hysteresis loops exhibit an initial cyclic hardening phase followed by stabilised cyclic plasticity. This stabilisation is accompanied by progressive plastic strain accumulation and the steady growth of ductile damage, reflecting void nucleation and growth-driven fatigue degradation in CuCrZr under high-temperature cyclic loading. Failure occurs after 44 load cycles under the evaluated operating conditions.

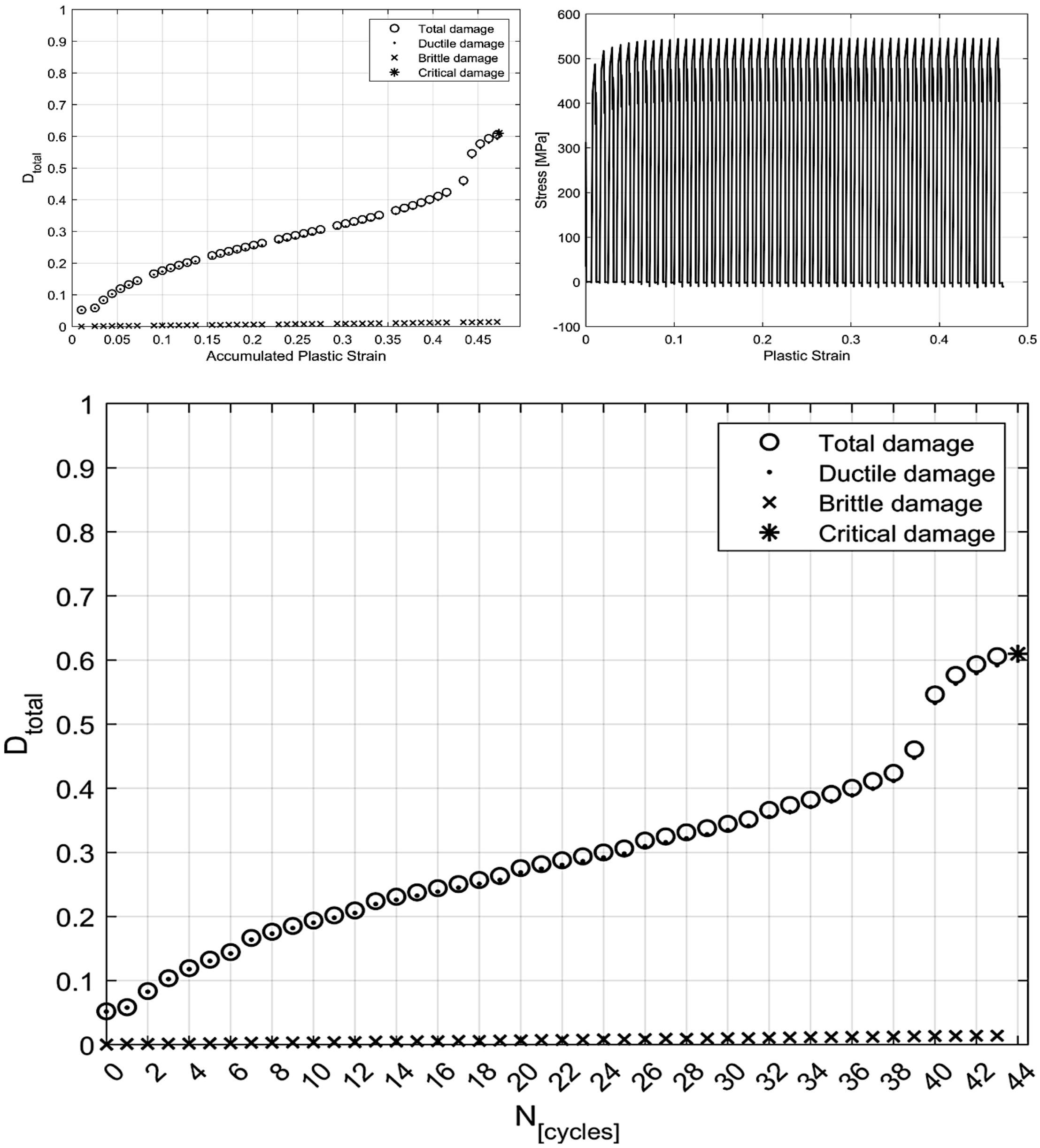

Figure 10 Damage evolution and stress–strain hysteresis in the combustion chamber liner throat region of a gas generator cycle engine

4. CONCLUSIONS

This study presents an integrated framework for evaluating the fatigue life of regeneratively cooled combustion chambers by linking transient engine-cycle simulations with thermo-structural finite element analysis and damage post-processing. By directly coupling engine-cycle-derived boundary conditions with fatigue evaluation, the methodology enables a cycle-consistent assessment of thermo-mechanical loading under representative operating conditions. The proposed approach supports efficient evaluation of reusability within system-level engine-cycle analysis at early design stages.

The predicted boundary conditions align with reported data for a Vulcain 2-class engine, demonstrating coupling between chamber pressure, propellant mass flow rate, and heat transfer throughout transient operation. This alignment confirms that the resulting thermo-mechanical response is driven by physically consistent engine conditions. The results indicate ductile-dominated fatigue behaviour, with the critical damage threshold reached after 44 load cycles under the evaluated conditions. When mapped to representative mission profiles, this corresponds to approximately 3–4 load cycles per mission, resulting in an estimated reusability of about 10 missions.

The analysis demonstrates how fatigue life is governed by engine-cycle-derived thermo-hydraulic boundary conditions, where imposed heat flux and coolant-side heat transfer control wall temperature gradients and drive the localisation of plastic strain in the throat region. This identifies the governing mechanism of damage accumulation and establishes a direct, quantitative link between engine-cycle operation and structural durability, demonstrating that the transient thermo-hydraulic conditions during the operating cycle determine the resulting fatigue life.

The framework employs a reduced-order engine-cycle representation and a quasi-2D structural model, enabling direct propagation of transient operating conditions into fatigue life prediction and allowing comparative evaluation of design choices at the system level. Computational efficiency is primarily achieved through post-processing damage evaluation, which avoids iterative coupling with the structural solution and eliminates the need for repeated finite element re-analysis, enabling rapid fatigue life assessment across varying operating conditions.

Future work will extend the framework to additional engine cycle configurations and improved thermal boundary condition representations to further refine fatigue life predictions.

Nomenclature

$D_{brittle}$	brittle damage component
D_{cr}	critical damage threshold
$D_{ductile}$	ductile damage component
D_{total}	total damage
E	Young's modulus
F_{sl}	sea-level thrust
h_{th}	heat transfer coefficient at throat
$I_{sp,sl}$	sea-level specific impulse
$\dot{m}$	mass flow rate
MR	mixture ratio
p	pressure
p_c	combustion chamber pressure
$p_{cool,th}$	coolant pressure at throat
$p_{p,f}$	fuel pump outlet pressure
$p_{p,ox}$	oxidiser pump outlet pressure
q''	heat flux
$R_{v,i}$	stress triaxiality at increment i
S	material fitting parameter
s	material parameter for damage evaluation
t_{wall}	wall thickness
T_c	combustion chamber temperature
$T_{cool,th}$	coolant temperature at throat
T_{gg}	gas generator temperature
$T_{w,cold}$	cold-side wall temperature
$T_{w,hot}$	hot-side wall temperature
$\varepsilon_{elastic}$	elastic strain
ε_f	failure strain
$\varepsilon_{plastic}$	plastic strain
ε_{th}	damage threshold strain
$\varepsilon_{(i+1)}$	strain at increment i+1
$\sigma_{eq,i}$	equivalent stress at increment i
σ_x	normal stress in x-direction
Δt_i	time increment
α	damage exponent

5. REFERENCES

1. Hetnarski RB. Encyclopedia of Thermal Stresses. Encyclopedia of Thermal Stresses. 1st ed. Springer Dordrecht; 2014. doi:https://doi.org/10.1007/978-94-007-2739-7
2. Sam L, Idithsaj PT, Nair PP, Suryan A, Narayanan V. Prospects for scramjet engines in reusable launch applications: A review. Int J Hydrogen Energy. 2023;48(92):36094–111. doi:https://doi.org/10.1016/j.ijhydene.2023.05.341
3. Gulczyński MT, Vennitti A, Scarlatella G, Dominguez Calabuig GJ, Blondel-Canepari L, Weber F, et al. RLV applications: challenges and benefits of novel technologies for sustainable main stages. In: Proceedings of the International Astronautical Congress, IAC [Internet]. Dubai: International Astronautical Federation, IAF; 2021. p. 1–20. Available from: https://elib.dlr.de/148758/
4. Bäker M, Fiedler T, Rösler J. Stress

evolution in thermal barrier coatings for rocket engine applications. Mech Adv Mater Mod Process. 2015;1(1):5. doi:10.1186/s40759-015-0005-2
5. Babu A, Asraff AK, Philip N. Fatigue Life Prediction of a Rocket Combustion Chamber. IOSR Journal of Mechanical and Civil Engineering. 2014;11(5):12–20. doi:10.9790/1684-11521220
6. Gulczyński MT, Riccius J, Deeken JC, Oschwald M. Optimized Postprocessing Method for Fatigue Life Evaluation of Reusable Rocket Combustion Chambers. J Propuls Power. 2026 Jan;42(1):134–48. doi:10.2514/1.B39921
7. Gulczynski MT, Riccius JR, Waxenegger-Wilfing G, Deeken J, Oschwald M. Combustion Chamber Fatigue Life Analysis for Reusable Liquid Rocket Engines (LREs). In: AIAA SCITECH 2023 Forum [Internet]. Reston, Virginia: American Institute of Aeronautics and Astronautics; 2023. Available from: https://arc.aiaa.org/doi/10.2514/6.2023-1263 doi:10.2514/6.2023-1263
8. Gulczyński MT, Riccius JR, Waxenegger-wilfing G, Deeken JC, Oschwald M. Numerical Fatigue Life Analysis of Combustion Chamber Walls for Future Reusable Liquid Rocket Engines (LREs) Applications. In. ESTORIL, PORTUGAL: Space Propulsion Conference; 2022. p. 1–14.
9. Zhang W. Failure characteristics analysis and fault diagnosis for liquid rocket engines. Failure Characteristics Analysis and Fault Diagnosis for Liquid Rocket Engines. 2016. 1–401 p. doi:10.1007/978-3-662-49254-3
10. Liu Y, Li X, Wang P, Zhang X, Zhu H, Cai G. Multi-Objective, Multi-Disciplinary Design Optimization and Multi-Attribute Evaluation of Hybrid Rocket Motors Used for Manned Lunar Lander. Aerospace. 2023;10(3). doi:10.3390/aerospace10030272
11. Qi Y, Jin P, Chen Z, Lv J, Cai G. Thermal-structural analysis for reusable thrust chamber using temperature-dependent CuZr alloy model adapted to cryogenic to elevated temperature. Aerosp Sci Technol. 2024;145:108782. doi:https://doi.org/10.1016/j.ast.2023.108782
12. Kringe PH, Riccius JR, Hardi J, Oschwald M, Gernoth A, Soller S, et al. Experimental and Numerical Fatigue Life Study of Inner Liner Material in Rocket Combustion Chambers. IEEE Aerospace Conference Proceedings. 2023;2023-March. doi:10.1109/AERO55745.2023.10115623
13. Gulczyński MT, Hahn RHS, Waxenegger-Wilfing G, Deeken JC, Oschwald M. Parametric Optimization of Turbopump for Reusable Rocket Engine (RRE) Applications. In: 34th International Symposium on Space Technology and Science [Internet]. Kurume in Fufkuoka,JAPAN; 2023. p. 10. Available from: https://archive.ists.ne.jp
14. H. S. Hahn R, Gulczyński MT, Kurudzija E, Dresia K, Waxenegger-Wilfing G, Deeken J. LUMEN EVOLUTION FOR LUNAR LANDER PROPULSION. In. ESA, FAR Conference 2022; 2022.
15. Gulczyński MT, Hahn RHS, Deeken JC, Oschwald M. Turbopump Parametric Modelling and Reliability Assessment for Reusable Rocket Engine Applications. Aerospace. 2024;11(10). doi:10.3390/aerospace11100808
16. Gulczyński MT, Riccius JR, Waxenegger-Wilfing G, Deeken JC, Oschwald M. Turbine Blades for Reusable Liquid Rocket Engines (LRE) – Numerical Fatigue Life Investigation. In: IEEE Aerospace Conference. Big Sky: IEEE; 2023. p. 10.1109/AERO55745.2023.10115912. doi:10.1109/AERO55745.2023.10115912
17. Gulczyński MT, H. S. Hahn R, Riccius JR, Zametaev EB, Waxenegger-wilfing G, Deeken JC, et al. Numerical Turbine Blade Fatigue Life Analysis for Reusable Liquid Rocket Engines (LREs) Applications. In. 2022. p. 1–14. doi:10.13009/EUCASS2022-6150
18. Pizzarelli M, Nasuti F, Onofri M. Trade-off analysis of high-aspect-ratio-cooling-channels for rocket engines. Int J Heat Fluid Flow. 2013 Dec;44:458–67. doi:10.1016/j.ijheatfluidflow.2013.08.003
19. Jin P, Lv J, Peng Q, Zhang H, Cai G, Zhou J. An analytical formula evolved from thermal-structural coupling model for life prediction and structural design of reusable thrust chambers. Appl Therm Eng. 2024 Aug 15;251. doi:10.1016/j.applthermaleng.2024.123568
20. LIU D, SUN B, WANG T, SONG J, ZHANG J. Thermo-structural analysis of regenerative cooling thrust chamber cylinder segment based on experimental data. Chinese Journal of Aeronautics. Chinese Journal of Aeronautics; 2020. p. 102–15. doi:10.1016/j.cja.2019.09.023
21. Martin MA, Nguyen HH, Greene WD, Seymour DC. Transient Mathematical Modeling for Liquid Rocket Engine Systems: Methods, Capabilities, and Experience. 2003.
22. Miao X, Hu J, Fu R, Xu Y, Luo P, Yang J, et al. Thermo-mechanical response characteristics of a novel node-integrated lattice sandwich thrust chamber structure under coupled thermal and mechanical fields. International Communications in Heat

and Mass Transfer. 2026 Mar 1;172. doi:10.1016/j.icheatmasstransfer.2025.110206
23. Sutton GP, Biblarz O. Rocket Propulsion Elements. Ninth Edit. John Wiley & Sons; 2016.
24. Kitsche W. Operation of a Cryogenic Rocket Engine. Vol. 2. 2010. doi:10.1007/978-3-642-10565-4
25. Coulon D. European Space Agency www.esa.int/ [Internet]. [cited 2025 Aug 7]. p. 123–4. Vulcain-2 Cryogenic Engine Passes First Test with New Nozzle Extension. Available from: https://www.esa.int/esapub/bulletin/bullet102/Coulon102.pdf
26. SONG J, SUN B. Thermal-structural analysis of regeneratively-cooled thrust chamber wall in reusable LOX/Methane rocket engines. Chinese Journal of Aeronautics. 2017;30(3):1043–53. doi:https://doi.org/10.1016/j.cja.2017.04.007
27. Lagier R. Ariane 5 User's Manual Issue 5 Revision 2 [Internet]. 2016 Oct. Available from: www.arianespace.com
28. Vetcha N, Strickland MB, Philippart KD, Giel T V. Overview of RS-25 Adaptation Hot-Fire Test Series for SLS, Status and Lessons Learned. In. AIAA; 2018 [cited 2025 Jul 11]. Available from: https://ntrs.nasa.gov/api/citations/20180006338/downloads/20180006338.pdf doi:https://doi.org/10.2514/6.2018-4459
29. Ellerbrock H. ASTRIUM An EADS Company [Internet]. [cited 2025 Jan 7]. p. 1–4. Vulcain 2: Thrust Chamber. Available from: https://www.yumpu.com/en/document/view/17516895/vulcain-2-thrust-chamber-eads
30. https://www.avio.com/component/vulcain-2-turbopump-main-characteristics [Internet]. [cited 2025 May 10]. VULCAIN 2 TURBOPUMP MAIN CHARACTERISTICS Avio S.p.A. Available from: https://www.avio.com/component/vulcain-2-turbopump-main-characteristics
31. Dufailly J, Lemaitre J. Modeling Very Low Cycle Fatigue. International Journal of Damage Mechanics. 1995. p. 153–70. doi:10.1177/105678959500400204
32. Bonora N, Gentile D, Pirondi A. Identification of the parameters of a non-linear continuum damage mechanics model for ductile failure in metals. Journal of Strain Analysis for Engineering Design. 2004;39(6):639–51. doi:10.1243/0309324042379356
33. Richardson MP. Reusable Rocket Engine Thrust Chamber Life Extension Analysis. [Tokyo]: The University of Tokyo; 2019.
34. Ivancic B. Industrial Aspects of Real Gas Phenomena and Challenges in Rocket Propulsion Engines [Internet]. London; 2022 Oct [cited 2025 Sep 12]. Available from: https://www.citystgeorges.ac.uk/__data/assets/pdf_file/0012/709698/Keynote1_Ivancic.pdf